

Requirements and limitations of imaging airway smooth muscle throughout the lung in vivo

Michael J. Hackmann^{a,b,*}, John G. Elliot^{a,c}, Francis H.Y. Green^d, Alvenia Cairncross^a, Barry Cense^{b,e}, Robert A. McLaughlin^{f,g,b}, David Langton^h, Alan L. James^{c,i}, Peter B. Noble^a, Graham M. Donovan^j

^a School of Human Sciences, The University of Western Australia, Crawley, Western Australia, Australia

^b School of Engineering, University of Western Australia, Perth, Western Australia, Australia

^c West Australian Sleep Disorders Research Institute, Department of Pulmonary Physiology and Sleep Medicine, Sir Charles Gairdner Hospital, Nedlands, Western Australia, Australia

^d Department of Pathology and Laboratory Medicine, Cumming School of Medicine, University of Calgary, Calgary, Alberta, Canada

^e Department of Mechanical Engineering, Yonsei University, Seoul, South-Korea

^f Australian Research Council Centre of Excellence for Nanoscale Biophotonics, Faculty of Health and Medical Sciences, The University of Adelaide, Adelaide, South Australia, Australia

^g Institute for Photonics and Advanced Sensing, The University of Adelaide, Adelaide, South Australia, Australia

^h Faculty of Medicine, Nursing and Allied Health, Monash University, Melbourne, Victoria, Australia

ⁱ Medical School, The University of Western Australia, Nedlands, Western Australia, Australia

^j Department of Mathematics, University of Auckland, Auckland, New Zealand

ARTICLE INFO

Keywords:

Airway smooth muscle
Remodeling
Asthma
Bronchoscopy
Imaging
Polarization-sensitive optical coherence tomography

ABSTRACT

Clinical visualization and quantification of the amount and distribution of airway smooth muscle (ASM) in the lungs of individuals with asthma has major implications for our understanding of airway wall remodeling as well as treatments targeted at the ASM. This paper theoretically investigates the feasibility of quantifying airway wall thickness (focusing on the ASM) throughout the lung in vivo by means of bronchoscopic polarization-sensitive optical coherence tomography (PS-OCT). Using extensive human biobank data from subjects with and without asthma in conjunction with a mathematical model of airway compliance, we define constraints that airways of various sizes pose to any endoscopic imaging technique and how this is impacted by physiologically relevant processes such as constriction, inflation and deflation. We identify critical PS-OCT system parameters and pinpoint parts of the airway tree that are conducive to successful quantification of ASM. We further quantify the impact of breathing and ASM contraction on the measurement error and recommend strategies for standardization and normalization

1. Introduction

Endoscopic polarization-sensitive optical coherence tomography (De Boer et al., 2017) is an effective tool for the visualization and quantification of airway smooth muscle (ASM) in a living individual (Adams et al., 2016; Li et al., 2018; Vaselli et al., 2020) and has the potential to provide

significant new insights in asthma research. Asthma is a chronic inflammatory condition of the lungs that affects 300 million people worldwide, with annually 250,000 deaths and 15 million disability-adjusted life years lost (Bateman et al., 2008; Asthma Australia and National Asthma, 2015). A primary pathology of asthma is remodeling of the airway wall, particularly hyperplasia and hypertrophy of the ASM (Ebina et al., 1993; James

Abbreviations: ASM, Airway smooth muscle; BT, bronchial thermoplasty; CT, Computed tomography; FA, Fatal asthma; FRC, Functional residual capacity; ID, Inner diameter; IW, Inner airway wall (includes mucosa and ASM); IWT, inner wall thickness; LL, Lower lobe; MRI, Magnetic resonance imaging; n , Refractive index; NA, Non-asthmatic control; NFA, Non-fatal asthma; OD, Outer diameter; P_{bm} , Perimeter of the basement membrane; P_L , Perimeter of the airway lumen as visible with PS-OCT; PS-OCT, Polarization-sensitive optical coherence tomography; P_{tm} , Transmural pressure; SD, Standard deviation; SNR, Signal-to-noise ratio; TLC, Total lung capacity; TV, Tidal volume.

* Correspondence to: School of Electrical, Electronic and Computer Engineering, Mailbag M018, 35 Stirling Highway, Crawley, WA 6009 Australia.

E-mail address: michael.hackmann@research.uwa.edu.au (M.J. Hackmann).

<https://doi.org/10.1016/j.resp.2022.103884>

Received 4 November 2021; Received in revised form 8 February 2022; Accepted 5 March 2022

Available online 15 March 2022

1569-9048/© 2022 Elsevier B.V. All rights reserved.

et al., 2012). Thickening of the ASM layer exists in many but not all patients with asthma, and is variably distributed throughout the bronchial tree of affected individuals (Elliot et al., 2015). Specific treatment of airway remodeling can be considered through application of bronchial thermoplasty (BT), producing a heat-induced ablation of the ASM layer (Castro et al., 2010; Donovan et al., 2020). However, in clinical practice, there is currently no assessment of whether the small number of conducting airways treated with BT (approximately 20 out of 30,000) have excessive ASM, which likely contributes to heterogeneity in the response to BT (Pretolani et al., 2017). The lack of clinically available imaging tools to visualize the ASM limits the uptake and effectiveness of treatments like BT that target ASM.

The current gold standard for the in vivo assessment of ASM is biopsy, which is not only invasive, but also unable to provide more than a fractional view of the highly variable distribution of ASM throughout the lung (Doberer et al., 2015). There is an unmet need for imaging tools that are able to map the ASM distribution in small and large airways. Such tools would also aid in understanding disease development and response to treatment in longitudinal studies.

Recently, endoscopic polarization-sensitive optical coherence tomography (PS-OCT) has been developed for pulmonary imaging, including quantification of the ASM (Adams et al., 2021, 2016; Feroldi et al., 2019). As in endobronchial ultrasound, PS-OCT uses a spinning probe inserted into an airway via a bronchoscope channel, producing cross-sectional and three-dimensional images of the airway as the probe rotates and translates. While traditional OCT provides scattering contrast similar to ultrasound (albeit at higher resolution), PS-OCT additionally contrasts tissue types based on their degree of organization and the orientation of fibrous structures. This type of imaging is well-suited to smooth muscle, which is highly organized and follows a well-defined circumferential orientation and therefore has potential to be delineated with high fidelity. Although use of PS-OCT to image ASM

has been shown as proof of principle and clinically in individual airways, no study has evaluated whether bronchoscopic-guided PS-OCT can be applied *throughout* the lung; what the limiting factors are; and how remodeling and the dynamic behavior of airways impact clinical utility. Understanding how the capabilities of PS-OCT fit to the requirements of imaging the airway wall tissue in airways of various sizes will help design appropriate and achievable studies and support the appropriate use of PS-OCT in pulmonary medicine.

In this study, we create a statistical representation of a human lung based on data from 2255 airways and apply a mathematical model to study the impact of dynamic changes to the airways due to breathing (radial and horizontal expansion) and ASM contraction. We assess potential limitations to bronchoscopic PS-OCT that may arise in a number of scenarios, including: (i) where the imaging range of a system (i.e. the maximum imaging distance between the probe and the region of interest) is insufficient for large airways; (ii) where the image depth penetration into tissue of a PS-OCT system is insufficient to image ASM thickness; (iii) where the resolution is insufficient to resolve thin ASM layers; and (iv) where controlled access to peripheral airways is impeded by the size of the bronchoscope. Unavoidable effects of breathing and ASM contraction or tone, as well as an eccentric position of the imaging probe within the lumen may further exacerbate existing limitations and are included in the analysis. We further assess the error of ASM quantification that arises from quiet breathing, deep breathing and ASM contraction and show avenues to a standardized approach to ASM measurement. If PS-OCT is to mature into a commonly used clinical tool, knowledge of its limitations is important to guide optimal usage of this technology by clinicians and system design by engineers.

2. Methods

This study uses data from our extensive human tissue biobank to

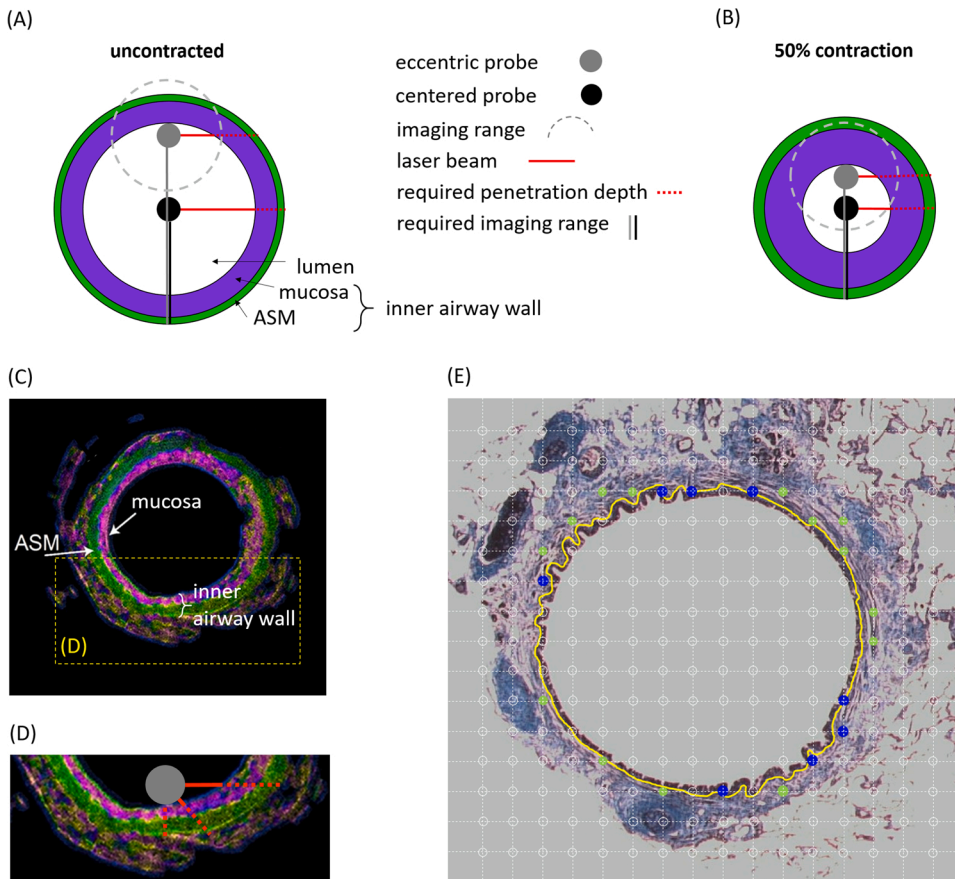


Fig. 1. (A) Schematic of the imaging geometry in an uncontracted airway with definitions of PS-OCT parameters, i.e. required penetration depth and imaging range. The imaging probe may be located in the lumen center (black circle) or eccentrically (gray circle), which impacts the feasibility of ASM imaging. (B) Schematic of the imaging geometry in a 50% contracted airway. (C) Representative PS-OCT image of an ex vivo porcine airway, showing mucosa and ASM tissue layers, which together make up the inner airway wall that the laser needs to penetrate in order to image the ASM. (D) Magnified image of the inset in (C) indicating an eccentrically positioned probe (gray circle). Note how the required penetration depth (length of the dotted red line) is impacted by the angle of the laser beam relative to the airway wall surface. (E) Representative human airway histological image (not corresponding to the porcine airway PS-OCT image). The lattice grid is used to quantify ASM area (green dots), mucosa (blue dots) and perimeter of the basement membrane (yellow line) by point counting (Green et al., 2010). Panels (C) and (D) adapted with permission (Li et al., 2019).

establish the thickness and variability of airway wall layers and how these change with airway size and asthma severity. To these data we apply an established mathematical model of airway compliance to simulate and study the impacts of airway dynamics. A representative lung geometry is used to establish which airways are accessible during bronchoscopic imaging.

2.1. Human lung specimens and morphometry

Methods for acquiring human airways are described in our previous publications (Donovan et al., 2018; Green et al., 2010; Hessel et al., 1999; Tough et al., 1996). In brief, left lungs were acquired from post-mortem cases classified as non-asthmatic control (NA, $n = 31$), with no history of asthma, wheeze, or other lung disease; nonfatal asthma (NFA, $n = 32$), death attributed to a non-respiratory cause and with a confirmed history of asthma; and fatal asthma (FA, $n = 25$), death attributed to asthma with a confirmed history. After fixation in glutaraldehyde, three segmental bronchi, two from the lower lobe (anterior and posterior basal) and one from the upper lobe (apical), were isolated from lung parenchyma. Portions of airway (free from parenchyma) were acquired at nine equidistant levels from proximal to distal locations, yielding 27 airways per subject. Samples were processed into wax blocks, sectioned (5 μm), and stained using the elastic trichrome technique.

The area of the ASM layer (ASM_{area}), the inner airway wall area (between the basement membrane and the outer border of the ASM layer) and the perimeter of the basement membrane (P_{bm}) were measured by point counting and linear intercept using a Nikon light microscope, drawing tube, and square lattice grid containing 240 points.

2.2. Mathematical model of airway structure

Since the ex vivo airway samples in the human tissue biobank have been prepared and quantified under conditions at higher pressure (20–40 cm H_2O), and airway dimensions including lumen size and airway wall thickness are subject to change with pressure, we use a mathematical model to adjust airway luminal sizes from the biobank dataset to conditions found during bronchoscopy, i.e., $P_{\text{tm}} = 5$ cm H_2O . Our model follows that of Lambert et al., which has been validated against data from excised human lungs (Lambert et al., 1982). The airway lumen radius r_i depends on the transmural pressure P_{tm} as well as the maximal radius $r_{i,\text{max}}$, the null-pressure radius R_i at $P_{\text{tm}} = 0$ and the parameters P_1, n_1, P_2, n_2 , which depend on the airway order (see Table S.1 in Supplemental material of (Politi et al., 2010)).

$$r_i^2 = R_i^2 (1 - P_{\text{tm}}/P_1)^{-n_1} \quad \text{for } P_{\text{tm}} \leq 0.$$

$$r_i^2 = r_{i,\text{max}}^2 - (r_{i,\text{max}}^2 - R_i^2) (1 - P_{\text{tm}}/P_2)^{-n_2} \quad \text{for } P_{\text{tm}} \geq 0.$$

Once the airway radius at the desired pressure is known, we add simple ASM contraction in the form of percent ASM shortening to the model, such that the contraction factor $c \in [0 \leq c \leq 1]$ linearly scales the radius of the lumen: $r_{\text{contracted}} = c \cdot r_{\text{uncontracted}}$. A 50% contraction induced by ASM then equals halving of the airway lumen. The Lambert model does not account for changes in airway length due to breathing pressures, but length changes do affect wall thickness. Therefore, we additionally model the effect of longitudinal stretch based on the substantiated assumption that the volume of the mucosal- and ASM layers in a given airway segment are constant over moderate longitudinal stretches (Khangure et al., 2004). The cross-sectional inner wall area of a stretched airway is then $A_{\text{stretched}} = A_{\text{unstretched}} \cdot L_{\text{unstretched}} / L_{\text{stretched}}$ and we assumed a cube-root relationship between lung volume and airway length changes (Hughes et al., 1972). Finally, knowledge of the lumen radius, mucosal area and ASM area allowed reconstruction of the ASM layer thickness and inner wall thickness (which includes mucosa and ASM) under the assumption of circularly symmetric morphology or homogeneous layer thickness (see Fig. 1).

2.3. Penetration depth and imaging range analysis

Imaging of the entire ASM by PS-OCT requires that the airway is neither too large in lumen, nor its wall too thick for the light to penetrate to the deeper boundary of the ASM. Both the required imaging range (i.e. the maximum distance between the probe and furthest part of the ASM) and required penetration depth (i.e., the maximum tissue thickness along the beam path) become increasingly challenging for an eccentrically positioned probe (see Fig. 1). In the case of a centered probe in a cylindrical section of airway, the required penetration depth equals the tissue thickness, while for an eccentric probe it is impacted by the relative angle of the imaging light beam to the airway wall surface, as well as on the relative sizes of probe and lumen. To generate the required penetration depth data, we recreated airways on a fine mesh of 3000×3000 pixels using the lumen diameter and inner wall thickness data using MATLAB (R2017b, Natick, Massachusetts, The MathWorks Inc.). We added a probe of 1.2 mm outer diameter (OD) in maximally eccentric position, drew the beam path for every angle of probe orientation in one degree increments and measured the distance through the inner wall. The maximum was then noted as the required penetration depth for that airway. The required imaging range for an eccentric probe position was simply calculated as the luminal diameter d minus half the probe diameter multiplied by the refractive index of air ($n_{\text{air}} = 1$), plus the product of the inner wall thickness and the tissue refractive index (n_{tissue}), which was assumed to be 1.36.

$$\text{required imaging range} = \left(d - \frac{OD}{2} \right) \cdot n_{\text{air}} + IWT \cdot n_{\text{tissue}}$$

Factoring in the refractive index is necessary since OCT by default measures optical path length, not distance. For airways of 1 mm diameter the probe of 1.2 mm diameter was assumed to stretch the lumen to fit (see Fig. 4).

2.4. Assessing spatial constraints of PS-OCT guided bronchoscopy

To create a lung model that indicates which (and how many) airways are accessible to PS-OCT via bronchoscopy we assumed an underlying lung geometry detailed in our previous work (Donovan et al., 2020). In short, the lung geometry for the large airways up to the first sub-segmental branching point was derived from CT imaging data in the literature (Clark et al., 2014; Hedges et al., 2015). Airways smaller than the resolution limit of CT were then added using a volume-filling algorithm (Tawhai et al., 2004), where the properties of each airway are based on its Horsfield order and drawn randomly from statistical distributions for that order. Such algorithmically generated models of the conducting airways have been shown to match well with branching characteristics measured in human lungs (Howatson Tawhai et al., 2000). We then deemed ‘repeatably accessible’ airways as those larger than the outer diameter of the bronchoscope, but also allowed for the PS-OCT probe to be advanced from the scope into the next bifurcation. One or two additional daughter airways are thus repeatably accessible for each parent airway that limits bronchoscope access (see Table 3). Accessibility of large and small airways was then compared for four of the most common bronchoscopes.

2.5. Quantification error calculations

Quantification errors of airway dimensions originating from both radial and longitudinal stretching of airways were calculated for absolute and normalized ASM quantities (see Table 4). Radial stretch was simulated using our mathematical model of airway compliance, by comparing airway dimensions at two points, e.g., after inhalation and exhalation (for quiet breathing and deep breathing), as well as before and after ASM contraction, under the assumption of conserved wall volume. Quiet breathing was defined as breathing between FRC and FRC+TV (equivalent to transmural pressures (P_{tm}) of 5 cm H_2O and 8

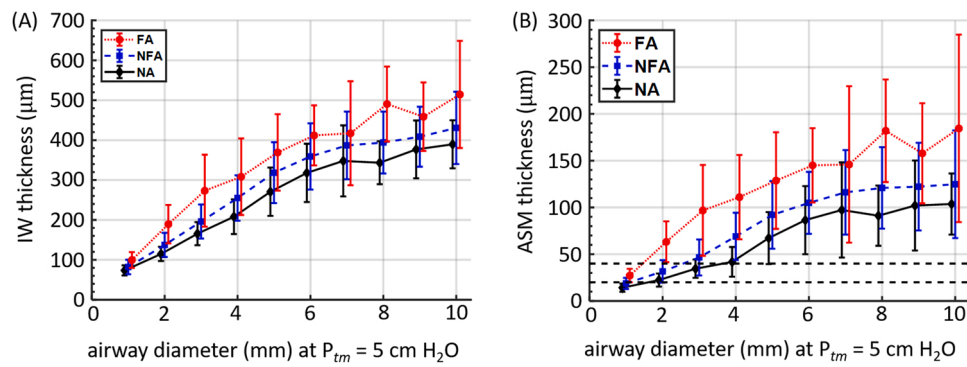


Fig. 2. (A) Inner wall thickness vs airway diameter. The inner wall comprises the mucosa and ASM layer, as illustrated in Fig. 1. (B) ASM thickness vs airway diameter. FA: fatal asthma (red), NFA: non-fatal asthma (blue), NA: no asthma (black). Sample sizes N for each data point are given in Table 1. Airways with diameters in a range of ± 0.5 mm were averaged. Black horizontal lines represent the 20–40 μm soft limit of PS-OCT resolution. Data are mean \pm SD.

Table 1
Sample size N for data on airway wall layer thickness data (cf. Fig. 2 and Table 2).

	$\varnothing = 1$ mm	2 mm	3 mm	4 mm	5 mm	6 mm	7 mm	8 mm	9 mm	10 mm
FA	162	125	95	62	46	35	27	36	33	15
NFA	190	167	151	90	57	41	35	36	31	22
NA	168	156	132	78	76	52	43	33	34	27

cmH₂O). Deep breathing was defined as breathing between FRC and TLC (equivalent to P_{tm} of 5 cmH₂O and 30 cmH₂O). Longitudinal stretching effects were calculated as proportional to the change in the cube-root of the lung volume (Prakash and Hyatt, 1978). Contraction of the ASM was assumed to alter only radial dimensions of airways.

3. Results and discussion

In Sections 3.1 and 3.2 we report airway wall layer thicknesses and compare imaging requirements to the limitations of PS-OCT. Section 3.3 describes the practical limitations of PS-OCT via bronchoscopy and in Section 3.4 we assess sources of quantification errors and provide solutions via standardization and normalization.

3.1. Airway wall layer thickness in human subjects

To understand the requirements for PS-OCT or any suitable imaging method, it is useful to first understand the structure of the ASM. The ASM band is located beneath the mucosal layer, which includes the epithelium, basement membrane and lamina propria. Both the ASM and the inner wall thickness (IWT) increase with airway size and asthma severity, as well as varying within and between individuals. We assess the capabilities of PS-OCT relative to an ‘average lung’ generated from a cohort of human lungs for each disease status (NA, NFA, FA).

The range of mean ASM thickness was $14 \pm 7 \mu\text{m}$ (NA, for airway diameter = 1 mm) to $185 \pm 100 \mu\text{m}$ (FA, for airway diameter = 10 mm) and the ASM was located between $74 \pm 13 \mu\text{m}$ and $514 \pm 134 \mu\text{m}$ from the luminal surface of the airway wall (Fig. 2). An imaging resolution of the order of a few micrometers is therefore required to resolve the finest ASM structures. While PS-OCT systems typically have an axial resolution of 5–10 μm , spatial averaging is often applied to improve the signal-to-

Table 2
ASM thickness (mean \pm SD, in μm) vs airway diameter (mm).

	$\varnothing = 1$ mm	2 mm	3 mm	4 mm	5 mm	6 mm	7 mm	8 mm	9 mm	10 mm
FA	$27 \pm 7^*, \dagger$	$63 \pm 22^*, \dagger$	$97 \pm 49^*, \dagger$	$111 \pm 45^*, \dagger$	$129 \pm 52^*, \dagger$	$145 \pm 40^*, \dagger$	146 ± 84	$182 \pm 55^*, \dagger$	$156 \pm 53^*$	185 ± 100
NFA	$19 \pm 6^*$	$32 \pm 12^*$	$47 \pm 19^*$	$69 \pm 25^*$	$92 \pm 36^*$	105 ± 33	116 ± 45	121 ± 44	122 ± 47	125 ± 58
NA	14 ± 4	22 ± 7	35 ± 10	42 ± 26	67 ± 28	86 ± 36	97 ± 51	91 ± 32	102 ± 48	104 ± 33

Comparisons of ASM thickness were made by mixed-effects (asthma severity and airway size) analysis,

* $p < 0.05$ vs NA, $\dagger p < 0.05$ vs NFA

noise ratio (SNR), to the detriment of spatial resolution. A recent PS-OCT study found reliable ASM quantification in animal models for ASM layers as thin as 20–40 μm (Adams et al., 2021). This suggests high suitability of PS-OCT for airways of 3–4 mm and larger, while still holding promise for airways even down to 1 mm diameter given realistic improvements in image resolution. Table 2 provides ASM thicknesses (mean \pm standard deviation (SD)) over a range of airway lumen sizes.

There were clear effects of asthma severity and airway size on ASM and IW thickness as commonly reported (Dunnill et al., 1969; James et al., 2012, 2009). On average, ASM thickness in the FA group was twice that of controls ($p < 0.001$) and in the NFA group ASM thickness was increased by 36% compared with controls ($p < 0.001$). Inner wall thickness was increased by 18% in the FA group ($p < 0.001$) and 9% in the NFA group compared ($p < 0.005$) with controls. Differences were less apparent in larger more proximally located airways, somewhat reflecting the reduced sample size at these locations. Mucosal thickness (IW thickness minus ASM thickness) increased with increasing airway diameter throughout all airway sizes.

3.2. Required penetration depth and imaging range

Imaging the ASM with PS-OCT requires that the polarized light travel from the probe through the lumen, mucosa and to the external border of the ASM, and then traverse the same distance back to be detected by the probe. The penetration depth of light into tissue that is required for a full circumferential measurement of the ASM depends on the tissue thickness and the light’s penetration angle. The former is a function of airway size (see Section 3.1), asthma severity, lung’s inflation state (breathing) and contraction of the ASM (tone). Penetration angle of light is influenced by the positioning of the probe within the airway lumen and the lumen shape (see Section 2.4). As Fig. 3 shows, an imaging method with a maximum

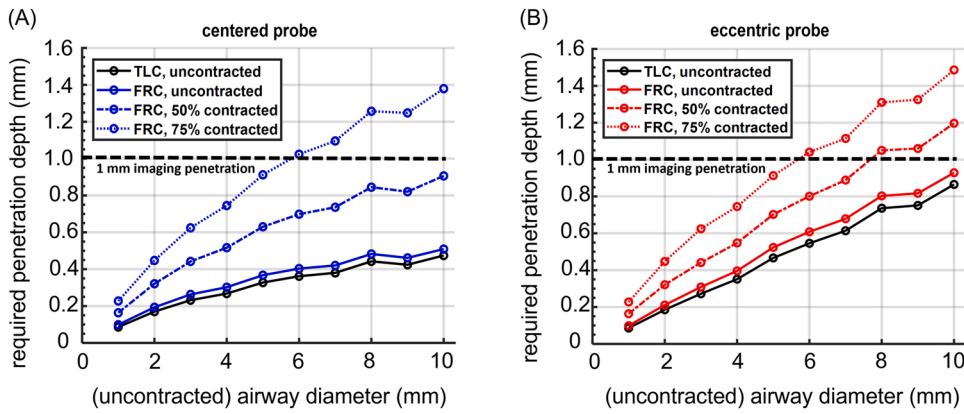


Fig. 3. The graphs show the penetration depth required to image the ASM at different stages of airway contraction, for centered (blue) and eccentric (red) positioning of the probe in the airway. ASM contraction substantially increases IW thickness and therefore the required penetration depth. The effects of deep breathing (FRC to TLC, solid lines) are negligible. (A) Centering the probe in the airway ensures that the required penetration depth does not exceed the limit of 1 mm (black dashed line) for uncontracted (blue solid line) and 50% contracted (blue dash dotted line) airways up to 10 mm baseline (uncontracted) diameter. In airways of more than 5 mm uncontracted diameter, excessive ASM contraction of 75% increases the required penetration depth beyond the 1 mm limit. (B) An eccentric probe position increases the required penetration depth (see also Fig. 1

(A) and 1(D)) substantially, although the added impact of ASM contraction is reduced compared to the case of a centered probe (see also Fig. 1(B)). Especially in large and/or contracted airways probe centering is important to ensure sufficient penetration depth to image the ASM. Data are shown only for the FA group as this poses the strictest requirement and differences between severity groups are small.

penetration depth of 1 mm can satisfy the requirement for a large range of lumen sizes and degrees of ASM contraction. This limit is robust against the impact of (quiet) breathing, eccentric probe positioning as well as ASM contraction of up to 50%, for all airways up to an uncontracted baseline diameter of 10 mm. When both eccentric probe position and 50% ASM contraction are present, airways up to 7 mm baseline diameter can still be examined for ASM content. Even at 75% ASM contraction airways up to 5 mm baseline diameter remain feasible. However, since the data points are based on the mean (of the FA group) there will be airways with thicker-than-average IW thickness that require an increased penetration depth. It is then useful to leverage central probe positioning and potentially use bronchodilators to relax contracted airways and thereby reduce ASM thickness.

Fig. 4 shows the effect of breathing, ASM contraction and probe position on the imaging range that is required to image the ASM across the circumference of the airway (see Section 2.4). Since the imaging range can be increased by technical means (albeit in a trade-off with resolution or digitization speed/cost) (An et al., 2013; Drexler and Fujimoto, 2015; Gora et al., 2009; Jing et al., 2012), it is less meaningful to assess this requirement against one fixed limit. Instead, the limits of systems that are published in the literature and have been applied to ASM imaging are used (Adams et al., 2016; Feroldi et al., 2019; Li et al., 2018). We note that in Fig. 4, the impact of breathing is negligible, while probe eccentricity plays a key role and can almost double the required

imaging range (compare red to blue lines), thereby quickly exceeding the capabilities of many PS-OCT systems. Contrarily, ASM contraction of 50% reduces the airway diameter and eases the imaging range requirement substantially. In that case, a system with 4 mm imaging range is sufficient for all airways up to 10 mm (uncontracted) baseline diameter, if the probe can be centered in the airway, by an experienced bronchoscopist. However, even in the worst case scenario of a probe in a maximally eccentric position with a limited imaging range, part of the ASM is often still imageable, although partial sampling holds the potential for unreliable results due to thickness variations around the airway – a fact that also limits the reliability of bioptic sampling (Doberer et al., 2015). For systems with limited imaging range, placing the probe adjacent to the airway wall is a viable strategy to at least partially sample larger airways. An analysis of the percentage of the ASM that is measurable under these circumstances can be found in Appendix A. Overall, an imaging range of less than 2–3 mm will considerably limit the applicability of the method, especially given the limited accessibility of small airways (see Section 3.3), while an imaging range of 10 mm enables PS-OCT assessment of ASM across the lung.

3.3. Assessing physical constraints of PS-OCT guided bronchoscopy

Besides the above technical limitations a further practical constraint is

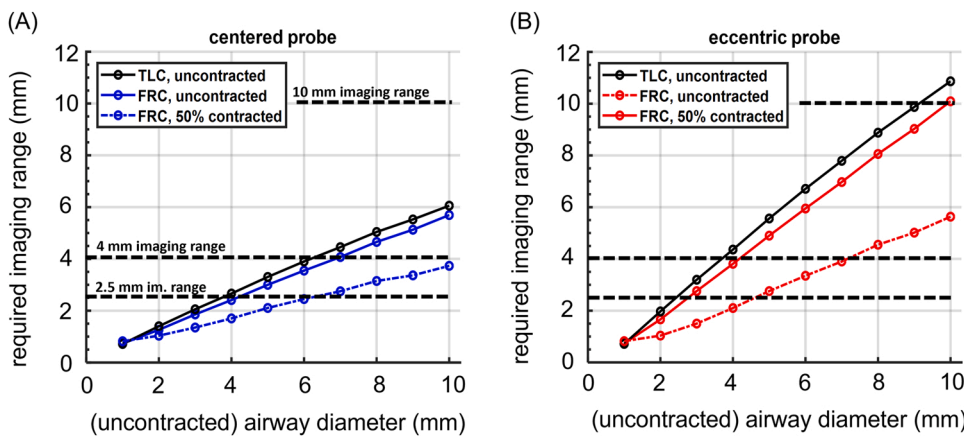


Fig. 4. The graphs show the imaging range required to visualize the ASM at different stages of airway contraction, for centered (blue) and eccentric (red) positioning of the probe in the airway. ASM contraction decreases the lumen diameter and therefore the required imaging range. The effects of deep breathing (FRC to TLC, solid lines) are negligible. (A) For PS-OCT systems with short imaging ranges, e.g. 4 mm, centering the probe in the airway ensures that the system can still be applied to large airways up to 6 mm diameter. (B) An eccentric probe position is a strong limiting factor for PS-OCT systems with short imaging ranges. In large airways probe centering may be controlled by bronchoscope positioning, while access to small airways may require pushing the PS-OCT probe far beyond the distal end of the bronchoscope, impeding the operator's control over probe centering. Data are shown only for the FA group

as this poses the strictest requirement and differences between severity groups are small. Imaging range limits of 2.5 mm, 4 mm and 10 mm are indicated by horizontal dotted lines, reflecting that of systems applied to airway imaging in the literature (Adams et al., 2016; Feroldi et al., 2019; Li et al., 2018).

Table 3

Specifications of commonly used bronchoscopes and resulting number of repeatably accessible airways in the left lung.

Model	Distal end outer diameter (mm)	Instrument channel diameter (mm)	Includes integrated video	Total repeatably accessible airways	Large (>2 mm) repeatably accessible airways	Small (<2 mm) repeatably accessible airways
BF-MP190F	3.0	1.7	yes	62–76	48	14–28
BF-P190	4.2	2	yes	39–48	All	None
BF-200	4.8	2	yes	25–32	All	None
BF-1TH190	6.2	2.8	yes	12–16	All	None

that not all airways in the lung are accessible via bronchoscopy. The outer diameter of the scope's distal end is a strong limitation for access to small airways (< 2 mm), with diameters of commonly used bronchoscopes ranging between 3 and 6 mm. Further requirements for the appropriate bronchoscope are the presence of an instrument channel that allows passing of the PS-OCT probe as well as video feedback. Commonly, endoscopic PS-OCT probes have diameters between 0.9 and 1.65 mm (Lee et al., 2014; Adams et al., 2019; Feroldi et al., 2019). Parameters of selected common bronchoscopes are summarized in Table 3.

Using our model of the bronchial tree (see Section 2.5) we assessed the impact of bronchoscope outer diameter on repeatable airway accessibility across the lung. This is relevant where the clinician is examining the effect of a targeted treatment on airway remodeling (e.g. BT) and the same airway must be assessed over time. We define repeatably accessible airways as those within reach of a bronchoscope and one branching generation beyond, since the PS-OCT probe is not in itself steerable but may be pushed from the scope and inserted into a bifurcation. In a representative lung, the number of accessible airways are shown in Table 3 and visualized in Fig. 5. Only the smallest available scopes allow any repeatable access to small airways (< 2 mm). Small airway disease is also a component of asthma and should be included in the assessment of a patient, emphasizing the need for small diameter bronchoscopes in PS-OCT based ASM quantification (Ueda et al., 2006).

Some smaller airways may be accessible randomly (i.e. non-repeatably) by pushing the PS-OCT probe far beyond the distal end of the scope. In our clinical experience this works well for up to 10 cm pushing distance, with the extent of access limited by the diameter and flexibility of the PS-OCT probe. External opaque CT scanning can be used to retain identification of the scanned airway, though repeatability of the insertion may be difficult, since the current PS-OCT endoscopes have no forward viewing feature and cannot be steered.

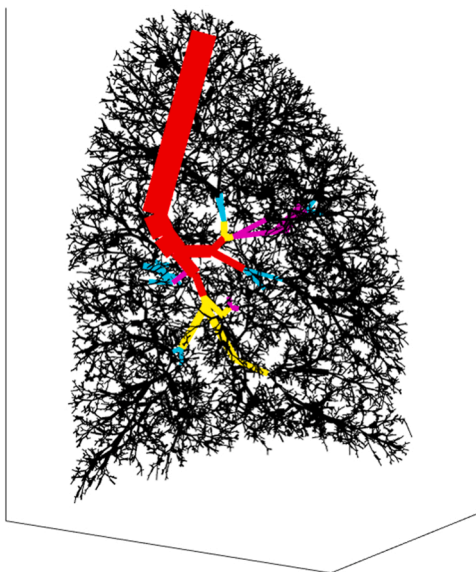


Fig. 5. Accessible airways when using different bronchoscopes of diameters: 6.2 mm (red), 4.8 mm (yellow), 4.2 mm (purple) and 3.0 mm (turquoise). Small footprint bronchoscopes are crucial for repeatable access to small airways.

3.4. Standardization and normalization of ASM quantification

When PS-OCT by means of bronchoscopy is performed, the ASM can be visualized. However, correct quantification still depends on the external conditions of the airway (such as inflation and contraction state), as well as the quantification techniques used for image analysis. The ASM may be quantified by different approaches, such as measuring either ASM thickness or area in individual radial cross-sectional images, or by measuring ASM volume in an airway segment. The lumen diameter and the area or thicknesses of mucosal- and ASM layers are subject to change during breathing and ASM contraction, which may give rise to a range of errors (see Table 4). The large differences between the measurement approaches in terms of their sensitivity to dynamic airways means that a standardized approach is necessary in order to compare results. Measuring the absolute cross-sectional ASM area is an acceptable method (4% error, see Table 4) during quiet breathing. Measuring the ASM volume in a given segment is a preferred approach as it leads to more robust measurements independent of the state of the airway (including contraction). In general, a sufficient length of airway needs to be sampled due to the potential for large local variations in ASM thickness (Adams et al., 2016).

In addition to quantifying the ASM it is important to correctly determine airway size, as defined by parameters such as diameter or perimeter. Airway size assessment is necessary in order for comparison of data between airways, subjects and time points, as well as for normalization, e.g., $\sqrt{\text{ASM}_{\text{area}}}/\text{perimeter}$. Presently, airway size is most commonly quantified by the dimension of the lumen in the OCT literature (Adams et al., 2016; Lee et al., 2014). However, asthmatic airways frequently have increased ASM tone (Ebina et al., 1993; James et al., 2012) and remain constricted to a smaller lumen size than non-asthmatic airways, such that matching and comparing airways based on this method will lead to an overestimation of ASM in asthmatic airways by mistakenly choosing larger, contracted airways (McParland et al., 2004). Conversely, normalization by the perimeter of the lumen P_L increases the measurement error (see Table 4) due to inflation, deflation and ASM contraction affecting P_L (Noble et al., 2010). In histological assessment, these issues are known and have been corrected by using the perimeter of the basement membrane P_{bm} instead of P_L . The P_{bm} of an airway remains mostly unchanged irrespective of contraction or dilation of the airway across moderate physiological conditions (James et al., 2008, 1988a, 1988b) and is therefore more suitable for normalization and comparison. If PS-OCT image quality can be improved to delineate the P_{bm} in airways, the measurements of airway wall thickness has the potential to be comparable between airways, subjects and time points.

The scale of the quantification errors can be comparable in magnitude to the change in ASM that is being quantified, which highlights the importance of correct normalization (i.e., using P_{bm}) and the adoption of standardized techniques for ASM quantification (i.e., using area or volumetric measurements). If breathing state cannot be fixed or controlled during measurement of an airway segment, then these errors will be innate in the measurement process. The errors arising if the patient is quietly breathing are relatively small and sedative drugs such as midazolam have been shown to reduce tidal volume but not FRC, which further reduces these errors (Gonzalez Castro et al., 2017; Morel et al., 1984). For deep breaths however, the errors become increasingly

Table 4

Percentage ASM quantification error. Dynamic changes in the airway due to breathing and ASM contraction cause (radial and longitudinal) stretching of the airway which impacts the measurement of ASM both in absolute terms and when normalized to the perimeter. Different measures of ASM quantity are affected differently. Where two separate errors are reported in one cell, these were calculated based on 1 and 10 mm diameter airways. Only one error is provided for some parameters, since these errors are independent of diameter. All values are in %.

	absolute ASM_{thickn}	normalized $\frac{ASM_{thickn}}{P_L}$	absolute ASM_{area}	normalized $\frac{\sqrt{ASM_{area}}}{P_L}$	absolute ASM_{vol}	normalized $\frac{\sqrt{ASM_{vol}}}{P_L \cdot L}$	lumen perimeter P_L
Quiet breathing	-10 to - 5	-17 to - 7	-4	-10 to - 4	0	-8 to - 2	+ 9 to + 2
Deep breathing	-30 to - 25	-42 to - 31	-20	-24 to - 17	0	-15 to - 7	+ 18 to + 8
50% ASM contraction	+ 50 to + 70	+ 200 to + 240	0	+ 100	0	+ 100	-50

significant and datasets acquired under such conditions should be considered with care, and potentially excluded, or techniques such as respiratory gating applied (McLaughlin et al., 2009). As a best practice, patient breathing (volume) should be monitored during PS-OCT.

3.5. Limitations of this study

The biobank data used in this study does not contain information on lumen shape or local variations in layer thickness. Reconstructing airways with our mathematical model assumes homogeneous wall thickness and airways were approximated as circularly symmetric cylinders. However, airway wall layer thickness can change along the circumference of the airway. In particular, mucosal folding may create local bulges that are thicker than the average mucosa (Wiggs et al., 1997). In practice, administration of a bronchodilator prior to PS-OCT may then be desirable to remove folding and reduce the required penetration depth to a level within the abilities of PS-OCT.

We note that ASM will deviate from the uniform thickness assumed within this study, as well as potentially only spanning part of the airway's circumference. While a fully circumferential ASM layer of non-uniform thickness implies regions with thinner-than-average ASM, the contrary scenario of a thicker layer intersected with gaps is also imaginable, causing thicker-than-average ASM. A further assumption is the absence of mucus in the airway. Although generally present, particularly in airways of subjects with asthma, mucus is translucent and may be cleared by bronchoscope suction. Image distorting effects of mucus or other fluids can potentially be corrected in PS-OCT post processing (Adams et al., 2019; Westphal et al., 2002).

Findings on limitations due to penetration depth are impacted by our assumption that the useful image penetration depth of PS-OCT is approximately 1 mm. The image penetration depth is limited by optical backscatter and absorption, resulting in attenuation of the signal in turbid tissue. While OCT is sometimes described as having a penetration depth of 2–3 mm in soft tissue, this is only possible in optically transparent tissues, which is not the case in the airway. Previous studies have suggested a useful image penetration of 1.5 mm for intensity-based OCT (Welzel, 2001). In our experience, the additional requirements in PS-OCT of reliably computing the change in polarization of the optical signal reduce this to 1 mm in practice.

4. Conclusions and recommendations

The current gold standard for the in vivo assessment of ASM is biopsy, which is not only invasive, it is also unable to provide more than a fractional view of the highly variable distribution of ASM throughout the lung (Doberer et al., 2015). PS-OCT offers a useful imaging approach to the task of mapping ASM distribution.

This study summarizes the requirements that any endoscopic imaging technique must meet in order to visualize the ASM in airways throughout the lung, such as sufficient resolution, imaging range, penetration depth and small footprint of the bronchoscopic probe. These requirements were assessed against data on the mean ASM thickness and variability in a large sample of the human population with and without

asthma. The presented data are a valuable resource and can serve as a benchmark to define airway wall remodeling, which is the target for bronchoscopic-guided PS-OCT. Thickness of ASM varies substantially between and within subjects (not shown), as well as with asthma severity, and ranged from a few micrometers (challenging for PS-OCT) up to several hundred micrometers.

In this paper, we have assessed the technical and practical limitations of endoscopic PS-OCT via bronchoscopy. We found that PS-OCT has the potential to assess ASM distribution over a wide range of airway generations. Eccentric probe positioning and ASM contraction were identified as potential confounding factors in ASM assessment. In particular, eccentric probe positioning has a very large impact on the required imaging ranging of a PS-OCT system.

Bronchoscope choice severely limits repeatable accessibility of small airways. We note that imaging of the small airways would benefit from development of bronchoscopes with smaller than currently available footprint. Representative Olympus bronchoscopes were chosen but further models and manufacturers exist, however in a similar size range. Given the smaller diameter of PS-OCT probes (down to < 1 mm) compared to ultrasound or BT probes, small working channel devices such as pediatric scopes are also suitable.

Errors on quantification of ASM due to dynamic behavior of airways can become significant where subjects are breathing deeply (i.e., FRC to TLC) or airways are contracted, but impact differently on various measures of ASM (e.g., thickness, area, volume). Generally, measuring the ASM volume in an airway segment is least sensitive to error while measuring cross-sectional ASM area contains only small errors (< 10%) provided that the subject is breathing quietly. Quantification of luminal perimeter is similarly sensitive to dynamic airway behavior and when used for normalization of ASM measurements, will substantially affect outcomes, especially in pre-contracted airways. We note that a robust way to categorize airways for longitudinal and inter-patient comparison is by using the perimeter of the basement membrane.

Validation studies of PS-OCT based ASM quantification against histology have demonstrated the modality's precision and accuracy, but have so far been based on static, ex vivo animal airways (Adams et al., 2021, 2016). Dynamic changes to airway length and diameter that will affect the measured ASM and lumen size will occur in the clinical setting and need to be taken into account to avoid systematic errors and confounding factors, especially where the magnitude of these errors is of the order of the effect one is seeking to study.

4.1. Summarizing the considerations above, we make the following recommendations

1. PS-OCT system development should consider the range of ASM thicknesses and airway sizes that are of interest for a study.
2. It is important to center the probe in large airways and those with thick airway walls to reduce instances where the PS-OCT system has insufficient image penetration in tissue. PS-OCT provides a penetration depth that is sufficient for airways up to an uncontracted diameter of 10 mm and beyond, but probe eccentricity and ASM

contraction will reduce the range of airway diameters that are amenable to imaging.

- For longitudinal studies of peripheral airways (requiring repeatable access to the same airway) it is essential to use bronchoscopes with the smallest available footprint (typically 3 mm distal diameter).
- For normalization and comparability across airways, time points and subjects, the perimeter of the basement membrane is an appropriate measure of airway size and is less subject to variation or other confounding factors than the visible luminal perimeter or luminal diameter.
- ASM should ideally be quantified in terms of ASM volume per airway segment, as this parameter is more robust to variation due to dynamics of breathing or ASM contraction than measurements of ASM area or thickness from a single radial cross-sectional image.
- PS-OCT offers the potential ability to visualize and quantify ASM throughout the lungs and offers a useful adjunct to biopsy. Bronchoscopists trained in use of EBUS will require only minimal additional training in PS-OCT due to the similarity in operation of the devices.

Funding

This work was supported by the National Australian Health and Medical Research Council (NHMRC Grant number APP1180854), the Australian Research Council (CE140100003), the University of Western Australia (UWA) University Postgraduate Award (UPA) and SIRF scholarship.

Acknowledgments

We would like to acknowledge the work done by our colleagues Qingyun Li, Karol Karnowski, Martin Villiger, Onur Çetinkaya and David D. Sampson to acquire the PS-OCT image. We are grateful to Clinical Prof. Shiobhain Mulrennan for permitting us to observe a live bronchoscopy.

Disclosures

R.A.M. is a co-founder and director of Miniprobes Pty Ltd., a company that develops novel optical imaging systems. Miniprobes Pty Ltd did not contribute to this study. The remaining authors have no competing interests to declare.

Appendix A. Percent visibility of ASM in case of eccentric probe positioning and varying imaging ranges

The figures below show the accessible percentage of the airway wall as a function of airway diameter and system imaging range. See appendix fig. A1.

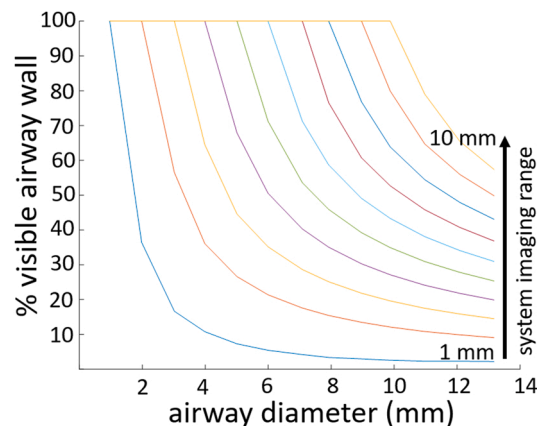
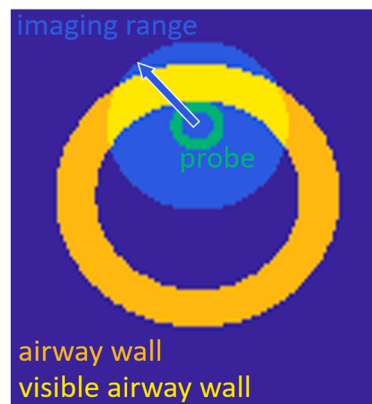


Figure (A1). Accessible percentage of the inner airway wall as a function of airway diameter and system imaging range.

References

- Adams, D.C., Hariri, L.P., Miller, A.J., Wang, Y., Cho, J.L., Villiger, M., Holz, J.A., Szabari, M.V., Hamilos, D.L., Harris, R.S., Griffith, J.W., Bouma, B.E., Luster, A.D., Medoff, B.D., Suter, M.J., 2016. Birefringence microscopy platform for assessing airway smooth muscle structure and function in vivo. *Sci. Transl. Med.* 8 <https://doi.org/10.1126/scitranslmed.aag1424> (359ra131-359ra131).
- Adams, D.C., Miller, A.J., Applegate, M.B., Cho, J.L., Hamilos, D.L., Chee, A., Holz, J.A., Szabari, M.V., Hariri, L.P., Harris, R.S., Griffith, J.W., Luster, A.D., Medoff, B.D., Suter, M.J., 2019. Quantitative assessment of airway remodelling and response to allergen in asthma. *Respirology* 1073–1080. <https://doi.org/10.1111/resp.13521>.
- Adams, D.C., Holz, J.A., Szabari, M.V., Hariri, L.P., Mccrossan, A.F., Manley, C.J., Fleury, S., O'Shaughnessy, S., Weiner, J., Suter, M.J., 2021. In vivo assessment of changes to canine airway smooth muscle following bronchial thermoplasty with OR-OCT. *J. Appl. Physiol.* 130, 1814–1821. <https://doi.org/10.1152/jappphysiol.00914.2020>.
- An, L., Li, P., Lan, G., Malchow, D., Wang, R.K., 2013. High-resolution 1050 nm spectral domain retinal optical coherence tomography at 120 kHz A-scan rate with 61 nm imaging depth. *Biomed. Opt. Express* 4, 245. <https://doi.org/10.1364/boe.4.000245>.
- Asthma Australia Council. National Asthma. The Hidden Cost of Asthma 2015 Deloitte Access Economics.
- Bateman, E.D., Hurd, S.S., Barnes, P.J., Bousquet, J., Drazen, J.M., FitzGerald, M., Gibson, P., Ohta, K., O'Byrne, P., Pedersen, S.E., Pizzichini, E., Sullivan, S.D., Wenzel, S.E., Zar, H.J., 2008. Global strategy for asthma management and prevention: GINA executive summary. *Eur. Respir. J.* 31, 143–178. <https://doi.org/10.1183/09031936.00138707>.
- Castro, M., Rubin, A.S., Lavolette, M., Fiterman, J., Lima, M.D.A., Shah, P.L., Fiss, E., Olivenstein, R., Thomson, N.C., Niven, R.M., Pavord, I.D., Simoff, M., Duhamel, D.R., McEvoy, C., Barbers, R., Ten Hacken, N.H.T., Wechsler, M.E., Holmes, M., Phillips, M.J., Erzurum, S., Lunn, W., Israel, E., Jarjour, N., Kraft, M., Shargill, N.S., Quiring, J., Berry, S.M., Cox, G., 2010. Effectiveness and safety of bronchial thermoplasty in the treatment of severe asthma: a multicenter, randomized, double-blind, sham-controlled clinical trial. *Am. J. Respir. Crit. Care Med.* 181, 116–124. <https://doi.org/10.1164/rccm.200903-0354OC>.
- Clark, A.R., Milne, D., Wilsher, M., Burrows, K.S., Bajaj, M., Tawhai, M.H., 2014. Lack of functional information explains the poor performance of “clot load scores” at predicting outcome in acute pulmonary embolism. *Respir. Physiol. Neurobiol.* 190, 1–13. <https://doi.org/10.1016/j.resp.2013.09.005>.
- De Boer, Johannes F., Hitzberger, Christoph K., Yasuno, Yoshiaki, 2017. Polarization sensitive optical coherence tomography – a review [Invited]. *Biomed. Opt. Express* 8, 1838–1873. <https://doi.org/10.1364/BOE.8.001838>.
- Doberer, D., Trejo Bittar, H.E., Wenzel, S.E., 2015. Should lung biopsies be performed in patients with severe asthma? *Eur. Respir. Rev.* 24, 525–539. <https://doi.org/10.1183/16000617.0045-2015>.
- Donovan, G.M., Elliot, J.G., Green, F.H.Y., James, A.L., Noble, P.B., 2018. Unraveling a clinical paradox: why does bronchial thermoplasty work in asthma? *Am. J. Respir. Cell Mol. Biol.* 59, 355–362. <https://doi.org/10.1165/rcmb.2018-0011OC>.
- Donovan, G.M., Langton, D., Noble, P.B., 2020. Phenotype- and patient-specific modelling in asthma: bronchial thermoplasty and uncertainty quantification. *J. Theor. Biol.* 501, 110337.
- Drexler, W., Fujimoto, J.G., 2015. Optical coherence tomography: Technology and applications, second edition, *Optical Coherence Tomography: Technology and Applications, Second Edition*. <https://doi.org/10.1007/978-3-319-06419-2>.
- Dunnill, M.S., Massarella, G.R., Anderson, J.A., 1969. A comparison of the quantitative anatomy of the bronchi in normal subjects, in status asthmaticus, in chronic bronchitis, and in emphysema. *Thorax* 24, 176–179. <https://doi.org/10.1136/thx.24.2.176>.
- Ebina, M., Takahashi, T., Chiba, T., Motomiya, M., 1993. Cellular hypertrophy and hyperplasia of airway smooth muscles underlying bronchial asthma: a 3-D morphometric study. *Am. Rev. Respir. Dis.* 148, 720–726. <https://doi.org/10.1164/ajrccm/148.3.720>.

- Elliot, J.G., Jones, R.L., Abramson, M.J., Green, F.H., Mauad, T., McKay, K.O., Bai, T.R., James, A.L., 2015. Distribution of airway smooth muscle remodelling in asthma: relation to airway inflammation. *Respirology* 20, 66–72. <https://doi.org/10.1111/resp.12384>.
- Feroldi, F., Willemse, J., Davidou, V., Graefe, M.G.O., van Iperen, D., Goorsenberg, A.W. M., Bonta, P.I., Annema, J.T., de Boer, J.F., 2019. In vivo multifunctional optical coherence tomography at the periphery of the lungs. *Biomed. Opt. Express* 10, 3070–3091.
- Gonzalez Castro, L.N., Mehta, J.H., Braynov, J.B., Mullen, G.J., 2017. Quantification of respiratory depression during pre-operative administration of midazolam using a non-invasive respiratory volume monitor. *PLOS One* 12, 1–11. <https://doi.org/10.1371/journal.pone.0172750>.
- Gora, M., Karnowski, K., Szkulmowski, M., Kaluzny, B.J., Huber, R., Kowalczyk, A., Wojtkowski, M., 2009. Ultra high-speed swept source OCT imaging of the anterior segment of human eye at 200 kHz with adjustable imaging range. *Opt. Express* 17, 14880. <https://doi.org/10.1364/oe.17.014880>.
- Green, F.H.Y., Williams, D.J., James, A., McPhee, L.J., Mitchell, I., Mauad, T., 2010. Increased myoepithelial cells of bronchial submucosal glands in fatal asthma. *Thorax* 65, 32–38. <https://doi.org/10.1136/thx.2008.111435>.
- Hedges, K.L., Clark, A.R., Tawhai, M.H., 2015. Comparison of generic and subject-specific models for simulation of pulmonary perfusion and forced expiration. *Interface Focus* 5. <https://doi.org/10.1098/rsfs.2014.0090>.
- Hessel, P.A., Mitchell, I., Tough, S., Green, F.H.Y., Cockcroft, D., Kepron, W., Butt, J.C., 1999. Risk factors for death from asthma. *Ann. Allergy, Asthma Immunol.* 83, 362–368. [https://doi.org/10.1016/S1081-1206\(10\)62832-3](https://doi.org/10.1016/S1081-1206(10)62832-3).
- Howatson Tawhai, M., Pullan, A.J., Hunter, P.J., 2000. Generation of an anatomically based three-dimensional model of the conducting airways. *Ann. Biomed. Eng.* 28, 793–802. <https://doi.org/10.1114/1.1289457>.
- Hughes, J.M.B., Hoppin, F.G., Mead, J., 1972. Effect of lung inflation on bronchial length and diameter in excised lungs. *J. Appl. Physiol.* 32.
- James, A.L., Pare, P.D., Hogg, J.C., 1988b. Effects of lung volume, bronchoconstriction, and cigarette smoke on morphometric airway dimensions. *J. Appl. Physiol.* 64, 913–919.
- James, A.L., Green, F.H., Abramson, M.J., Bai, T.R., Dolnikoff, M., Mauad, T., McKay, K. O., Elliot, J.G., 2008. Airway basement membrane perimeter distensibility and airway smooth muscle area in asthma. *J. Appl. Physiol.* 104, 1703–1708. <https://doi.org/10.1152/jappphysiol.00169.2008>.
- James, A.L., Bai, T.R., Mauad, T., Abramson, M.J., Dolnikoff, M., McKay, K.O., Maxwell, P.S., Elliot, J.G., Green, F.H., 2009. Airway smooth muscle thickness in asthma is related to severity but not duration of asthma. *Eur. Respir. J.* 34, 1040–1045. <https://doi.org/10.1183/09031936.00181608>.
- James, A.L., Elliot, J.G., Jones, R.L., Carroll, M.L., Mauad, T., Bai, T.R., Abramson, M.J., McKay, K.O., Green, F.H., 2012. Airway smooth muscle hypertrophy and hyperplasia in asthma. *Am. J. Respir. Crit. Care Med.* 185, 1058–1064. <https://doi.org/10.1164/rccm.201110-1849OC>.
- James, A.L., Hogg, J.C., Dunn, L.A., Paré, P.D., 1988. The Use of the Internal Perimeter to Compare Airway Size and to Calculate Smooth Muscle Shortening. *The American review of respiratory disease* 138, 136–139.
- Jing, J., Zhang, J., Loy, A.C., Wong, B.J.F., Chen, Z., 2012. High-speed upper-airway imaging using full-range optical coherence tomography. *J. Biomed. Opt.* 17, 110507. <https://doi.org/10.1117/1.jbo.17.11.110507>.
- Khangure, S.R., Noble, P.B., Sharma, A., Chia, P.Y., McFawn, P.K., Mitchell, H.W., 2004. Cyclical elongation regulates contractile responses of isolated airways. *Journal of applied physiology* 97 (3), 913–919. <https://doi.org/10.1152/jappphysiol.00262.2004>.
- Lambert, R.K., Wilson, T.A., Hyatt, R.E., Rodarte, J.R., 1982. A computational model for expiratory flow. *J. Appl. Physiol. Respir. Environ. Exerc. Physiol.* 52, 44–56. <https://doi.org/10.1152/jappphysiol.1982.52.1.44>.
- Lee, A.M.D., Kirby, M., Ohtani, K., Candido, T., Shalansky, R., MacAulay, C., English, J., Finley, R., Lam, S., Coxson, H.O., Lane, P., 2014. Validation of airway wall measurements by optical coherence tomography in porcine airways. *PLOS One* 9, 1–10. <https://doi.org/10.1371/journal.pone.0100145>.
- Li, Q., Karnowski, K., James, A., Villiger, M., Noble, P.B., Cairncross, A., Sampson, D.D., 2018. Robust reconstruction of local optic axis orientation with fiber-based polarization-sensitive optical coherence tomography. *Biomed. Opt. Express* 9, 5437. <https://doi.org/10.1364/boe.9.005437>.
- Li, Q., Karnowski, K., Noble, P.B., Hackmann, M., Çetinkaya, O., Cense, B., James, A., Villiger, M., Sampson, D.D., 2019. Local optic axis mapping for airway smooth muscle assessment in catheter-based polarization-sensitive optical coherence tomography (Conference Presentation). *Endosc. Microsc. XIV* 10854, 108540U.
- McLaughlin, R.A., Armstrong, J.J., Becker, S., Walsh, J.H., Jain, A., Hillman, D.R., Eastwood, P.R., Sampson, D.D., 2009. Respiratory gating of anatomical optical coherence tomography images of the human airway. *Opt. Express* 17, 6568. <https://doi.org/10.1364/oe.17.006568>.
- McParland, B.E., Paré, P.D., Johnson, P.R.A., Armour, C.L., Black, J.L., 2004. Airway basement membrane perimeter in human airways is not a constant; potential implications for airway remodeling in asthma. *J. Appl. Physiol.* 97, 556–563. <https://doi.org/10.1152/jappphysiol.00982.2003>.
- Morel, D.R., Forster, A., Bachmann, M., Suter, P.M., 1984. Effect of intravenous midazolam on breathing pattern and chest wall mechanics in humans. *J. Appl. Physiol. Respir. Environ. Exerc. Physiol.* 57, 1104–1110. <https://doi.org/10.1152/jappphysiol.1984.57.4.1104>.
- Noble, P.B., West, A.R., McLaughlin, R.A., Armstrong, J.J., Becker, S., McFawn, P.K., Williamson, J.P., Eastwood, P.R., Hillman, D.R., Sampson, D.D., Mitchell, H.W., 2010. Airway narrowing assessed by anatomical optical coherence tomography in vitro: dynamic airway wall morphology and function. *J. Appl. Physiol.* 108, 401–411. <https://doi.org/10.1152/jappphysiol.00511.2009>.
- Politi, A.Z., Donovan, G.M., Tawhai, M.H., Sanderson, M.J., Lauzon, A.M., Bates, J.H.T., Sneyd, J., 2010. A multiscale, spatially distributed model of asthmatic airway hyper-responsiveness. *J. Theor. Biol.* 266, 614–624. <https://doi.org/10.1016/j.jtbi.2010.07.032>.
- Prakash, U.B.S., Hyatt, R.E., 1978. Static mechanical properties of bronchi in normal excised human lungs. *J. Appl. Physiol. Respir. Environ. Exerc. Physiol.* 45, 45–50. <https://doi.org/10.1152/jappphysiol.1978.45.1.45>.
- Pretolani, M., Bergqvist, A., Thabut, G., Dombret, M.C., Knapp, D., Hamidi, F., Alavoine, L., Taillé, C., Chanez, P., Erjefält, J.S., Aubier, M., 2017. Effectiveness of bronchial thermoplasty in patients with severe refractory asthma: clinical and histopathological correlations. *J. Allergy Clin. Immunol.* 139, 1176–1185. <https://doi.org/10.1016/j.jaci.2016.08.009>.
- Tawhai, M.H., Hunter, P., Tschirren, J., Reinhardt, J., McLennan, G., Hoffman, E.A., 2004. CT-based geometry analysis and finite element models of the human and ovine bronchial tree. *J. Appl. Physiol.* 97, 2310–2321. <https://doi.org/10.1152/jappphysiol.00520.2004>.
- Tough, S.C., Green, F.H.Y., Paul, J.E., Wigle, D.T., Butt, J.C., 1996. Sudden death from asthma in 108 children and young adults. *J. Asthma* 33, 179–188. <https://doi.org/10.3109/02770909609054550>.
- Ueda, T., Niimi, A., Matsumoto, H., Takemura, M., Hirai, T., Yamaguchi, M., Matsuoka, H., Jinnai, M., Muro, S., Chin, K., Mishima, M., 2006. Role of small airways in asthma: investigation using high-resolution computed tomography. *J. Allergy Clin. Immunol.* 118, 1019–1025. <https://doi.org/10.1016/j.jaci.2006.07.032>.
- Vaselli, M., Feroldi, F., Willemse, J., Graefe, M.G.O., van Iperen, D., Goorsenberg, A.W. M., Bonta, P.I., Annema, J.T., de Boer, J.F., 2020. In vivo endoscopic multifunctional optical coherence tomography imaging of lungs periphery before and after bronchial thermoplasty. *EPJ Web Conf.* 238, 04002. <https://doi.org/10.1051/epjconf/202023804002>.
- Welzel, Julia (Department of Dermatology, Medical University of Luebeck, Luebeck, G., 2001. Optical coherence tomography in dermatology. *Ski. Res. Technol.* 7, 1–9. <https://doi.org/10.3109/9781420003307-38>.
- Westphal, V., Rollins, A., Radhakrishnan, S., Izatt, J., 2002. Correction of geometric and refractive image distortions in optical coherence tomography applying Fermat's principle. *Opt. Express* 10, 397. <https://doi.org/10.1364/oe.10.000397>.
- Wiggs, B.R., Hrousis, C.A., Drazen, J.M., Kamm, R.D., 1997. On the mechanism of mucosal folding in normal and asthmatic airways. *J. Appl. Physiol.* 83, 1814–1821. <https://doi.org/10.1152/jappphysiol.1997.83.6.1814>.